Fluid Dynamics & Materials Processing

Tech Science Press

DOI: 10.32604/fdmp.2022.021841

ARTICLE

Experimental Testing of Cellular Construction Materials Containing Flax Particles

Hamadou-Ali Mohamed[1,*], Benazzouk Amar[1,*], Haïkel Ben Hamed[1] and Arash Jamali[2]

[1]Laboratoire des Technologies Innovantes (UR-UPJV 3899)-UPJV, Amiens, 80000, France

[2]Plateforme de Microscopie Electronique-UPJV, HUB de l'Energie, 80039, Amiens

[*]Corresponding Authors: Hamadou-Ali Mohamed. Email: mohamed.hamadouali@outlook.com; Benazzouk Amar. Email: amar.benazzouk@u-picardie.fr

Received: 08 February 2022 Accepted: 24 March 2022

ABSTRACT

The feasibility of a sustainable non-autoclaved cellular concrete, based on flax vegetable co-products, for the production of usable specimen in the lightweight construction field, has been investigated experimentally. The produced specimen, containing various volume ratios of flax particles with respect to preformulatd Tradical PF70 lime binder of 0, 1, and 2, were lightened by creating a porous structure in the matrix through the addition of 0.3% wt. Aluminium powder (able to react with calcium hydroxide from the binder and result in microscopic air-bubbles). Fresh and hardened specimen properties, including hydration, fresh density, porosity, hardened density, compressive and flexural strengths, toughness energy, and dry thermal conductivity at different temperatures, were assessed for varying flax-to-binder ratios. Results have shown that the addition of Aluminum powder leads to restrain the setting time delay of binder-based lime. Moreover, the hardened material displays a significant decrease in specimen density, thereby resulting in a compressive strength level compatible with that required in the cellular construction materials sector. Results also highlighted the ability of added flax to induce a change in the specimen from brittle to ductile behavior. Moreover, a high degree of thermal insulation can be achieved, which makes the cellular specimen based on flax particle suitable as insulated-bearing walls material.

KEYWORDS

Flax particles; cellular concrete; lightening; porous structure; physico-mechanical properties; thermal conductivity

1 Introduction

Innovative building solutions for conserving non-renewable resources and to solve the problems related to environmental issues have motivated extensive research-works to develop eco-friendly sustainable building materials-based easily renewable natural raw material resources. In this context, a growing interest has been addressed on the addition of aggregates and fibers derived from vegetable materials into specimen called "green" concretes for eco-friendly constructions that meet the new requirements of users in terms of environmental concerns and comfort. In addition to its sustainable credentials, the use of vegetable materials exhibits a set of important advantages, such as wide availability at low cost, renewability, biodegradability, and low carbon footprint [1,2]. To promote specimen-based vegetable material in construction field, various types of vegetable species including flax, hemp, bamboo, coconut,

palm, kenaf, sisal, etc., were used to replace mineral aggregates and synthetic fibers in composite-mix to enhance specific characteristics of reinforced specimen and given rise to several applications [3–8]. The results have shown the efficiency of vegetable materials addition on the characteristics of reinforced composite specimen such as interesting physico-mechanical and thermo-hygric properties, reduction in the thermo-acoustic transfer, low density, and healthy living solutions.

In France, among a wide variety of vegetable sources, a great importance was accorded to hemp particles for their applications in construction sector. Considering as by-products derived from industrial hemp sector, these materials are becoming the subject of a major focus of the green housing sector because of their energy-efficient impact, and because hemp-based composites offer a high quality living environment. According to the works reported in the literature, several studies evidenced the benefits of concrete-based hemp particles as non-structural construction material, where the effect of different parameters like particle size, hydraulic and organic binder types, and casting process have been studied [9–15]. The results have promoted several potential applications of sample due to interesting properties such as a low density, high acoustic and thermal insulation performances, fire resistance, and higher hygro-thermal characteristics. In addition, the concrete-based hemp particles offers a healthy and high quality living environment, evidenced by the vegetable material capability to regulate indoor humidity of building by releasing and absorbing humidity [16–18]. In the same way, composite samples-based other vegetable-materials such as straw bales, rapeseed straw, corn stalk, jute straw, Diss, and rice husks mixed with different binder types have found to be energy efficient materials and provide concrete with high insulation properties [19–22]. Although the mentioned advantages of construction specimens-based vegetable particles, as regards energy saving and hygro-thermal performances, their use in hydraulic binder is limited by their low durability in alkaline environment, which results in their deterioration under mineralization and alkaline attacks mechanisms [23–25]. In addition the chemical compatibility between vegetable material and hydraulic binder is a still problem for specimen development, while the contained dissolved components composed by lignin, hemicellulose, terpenes, sugars, etc., inhibit binder hydration. It results in setting time delay which negatively affects the hardening of the specimen thus reducing its mechanical strengths development [26]. Therefore, the viability of using vegetable materials depends on their appropriate physical and/or chemical treatment [27,28].

Although the demand of vegetable materials is growing worldwide, the specimen-based these plants need further research. In this context, other alternative solution is to produce new cellular specimen-based flax materials usable in lightweight concrete construction. Depending to the production process, cellular concrete could reach a density range from 300 to 1,800 kg/m^3, compared to the traditional concrete which exhibits a density-value of approximately 2,300 kg/m^3. A further innovative strategy is the lightened of the specimen by creating a porous structure in the matrix. According to the researches down, these materials remain relatively unexplored. The main focuses of this study is to investigate the potentialities of use flax particles in preformulated Tradical PF70 hydraulic binder, in the objective to provide usable specimen in lightweight cellular material applications. The specimen was produced using Aluminum which reacts with calcium hydroxide to form air-bubbles in the matrix. The effect of flax particles to binder volume ratio varied from 0 (Control Specimen) to 2 on the fresh and hardened properties of cellular specimen was examined.

2 Materials and Experimental-Tests

2.1 Flax Particles

The vegetable particles used in this study are obtained from waste by-products materials, derived from textile linen industry textile and supplied by “La Calira”, in the Northern Region of France. Resulting from fibers stripping process and recovered within the dust extractor (exhauster hoods) these materials are composed of flax particles, steam fragments, and wood shaves, while the corresponding shape is shown in Fig. 1a. The gradation curve of flax products is reported in Fig. 1b, while the particles are less than 2 mm in size.

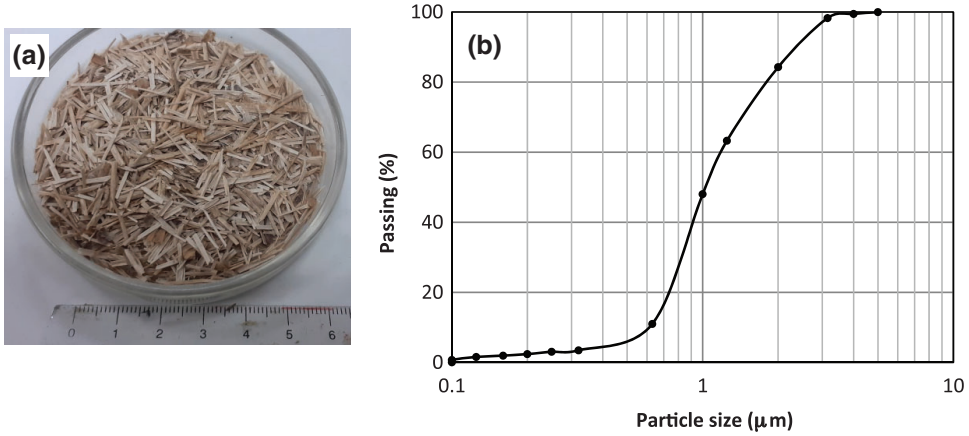

Figure 1: Shape and particle size distribution of flax particles

Several properties of flax particles including bulk and absolute densities, porosity and water absorption are analysed. The measurement of the bulk density of flax particles was determined by filling recipient of 1 Liter and weighing. The corresponding absolute density was evaluated by using the protocol described in the literature [22]. After milling in powder form, the particles were immersed in cyclohexane, while the measurement of its absolute density was carried out after reaching a constant volume of cyclohexane in the pycnometer, according to Eq. (1).

$$\rho_{abs} = \frac{M_D}{M_{D+C} - (M_C/\rho_C)} \tag{1}$$

where: ρ_C (kg/m^3) represents the density of cyclohexane, M_D, M_{D+C} and M_C (g) are the masses of hemp, pycnometer (cyclohexane + hemp), and cyclohexane, respectively.

The total porosity of used flax particles was determined as regards the obtained absolute and bulk density-values, according to Eq. (2) [29].

$$\varnothing = \left(1 - \frac{\rho_{bulk}}{\rho_{abs}}\right).100 \tag{2}$$

The water absorption amount was evaluated by total immersion of particles in water, after being dried the particles in a dry oven at 70°C before their immersion in tap water. After reaching a constant mass, the water absorption was determined considering the dry and total saturated masses of particles. The properties of flax particles are summarised in Table 1, where the reported-values are the average test-results of three replications.

Table 1: Properties of flax particles

Bulk density (kg/m^3)	Absolute density (kg/m^3)	Porosity (%)	Water absorption (%)
100 ± 10	1,054 ± 50	90.5 ± 12	280 ± 25

2.2 Preformulated Lime Binder-Based Tradical PF70

The preformulated lime binder used in this study, called "Tradical PF70" is supplied by "LHoist" industry, of the Northern Region of France [30]. It composed of 75% air lime, 10% hydraulic lime, and 15% of pozzolan mixture, where the binder is already used to produce hemp concrete.

The use of this binder has several advantages that are related to its hydrophobic nature which acts as protective barrier for included vegetable particles when specimen exposed to hygroscopic environment. The properties of Tradical PF70 binder are reported in Table 2.

Table 2: Properties of tradical PF70 based-binder [30]

Bulk density (kg/m^3)	Soluble silica (%)	CO_2 content (%)	Adjuvants (%)	Water retention (%)	Maximum grading size (mm)
720 ± 20	10 ± 2	8 ± 1	0.5 ± 0.02	75 ± 6	0.09

2.3 Mixing Procedure

Constituent materials mixes included air-lime based Tradical PF70 binder, Aluminum powder at 0.3% wt of binder, with 325 mesh in size and 99% purity, and flax particles to binder volume ratio of 0 (Control Specimen), 1 and 2. The interaction occurred between Aluminum powder and Calcium Hydroxide of lime binder produces hydrogen gas in the binder, and thus creates microscopic air bubbles in the matrix, according the chemical reaction mechanism:

$$2Al + 3Ca(OH)_2 + 6H_2O \longrightarrow 3CaO \cdot Al_2O_3 \cdot 6H_2O + 3H_2$$

Aluminum powder + Calcium Hydroxide Tricalcium Hydrate + Hydrogen

The specimen preparation was carried out by initially mixing Tradical PF70 binder and Aluminum powder in a mixer. After adding water, the required amount of flax particles was dispersed with slow increment throughout the fresh binder, to avoid a balling effect of vegetable particles. The obtained fresh specimen was then mixed for an additional two minutes at medium speed. After casting in the molds on a vibrating table, the fresh specimens were moist-cured for 28 days at 20 ± 2°C and 98% relative humidity. For hardened properties characterisation, prismatic, cylindrical, and parallelepiped samples of (40 × 40 × 160 mm), (110 × 220 mm), and (250 × 250 × 60 mm) in sizes were prepared for flexural and compressive tests, and thermal conductivity measurement, respectively. However, the expanded volume of fresh specimen that occurred after 20 min of casting due to the Aluminum powder and calcium hydroxide chemical reaction is shown in Fig. 2. The corresponding composition-mixes and designations of samples are summarized in Table 3.

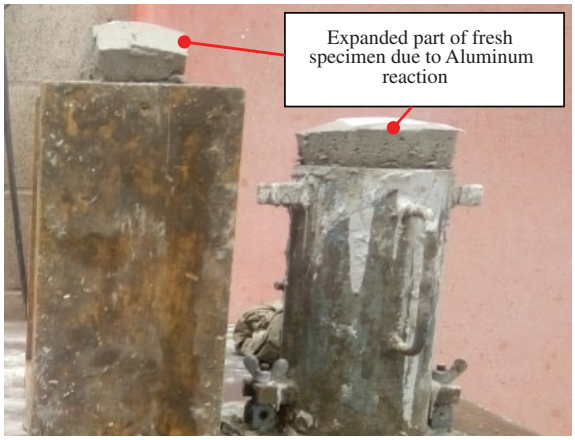

Figure 2: Shape of expanded fresh specimens

2.4 Experimental Testing

As mentioned previously, the suggested testing program focused on fresh and hardened properties of specimens. Given the chemical interaction issues reported in several research-works when using vegetable materials in hydraulic binders which usually results in delaying of setting time and hardening of specimen, it becomes necessary to examine the inhibitory effect exerted by flax particles on Tradical PF70 binder hydration after adding Aluminum powder. This step can be quantified through hydration-test of flax-binder mixture which leads to evaluate the inhibitory effect exerted by vegetable particles by examining the times of initial and final hydration reaction, maximum temperature reached during hydration, and the hydration rate. The test was conducted according to the procedure described by Moslemi et al. [31], where the experimental set-up and the schematic diagram of typical hydration curve are shown in Figs. 3a and 3b, respectively.

Table 3: Composition-mix and ID of reinforced specimens

Specimen-ID	Tradical PF70 binder (kg/m^3)	Flax particles (kg/m^3)	Aluminum/Binder ratio (%) (by mass)	Water/Binder ratio (by mass)
CC0F[a] (Control Specimen)	528	0	0.3	0.50
CC1F[b]	287	39.85	0.3	0.65
CC2F[c]	199	55.34	0.3	0.80

Notes: [a]Cellular concrete without flax; [b, c]Cellular concrete with 1 and 2 volume ratios of flax, respectively.

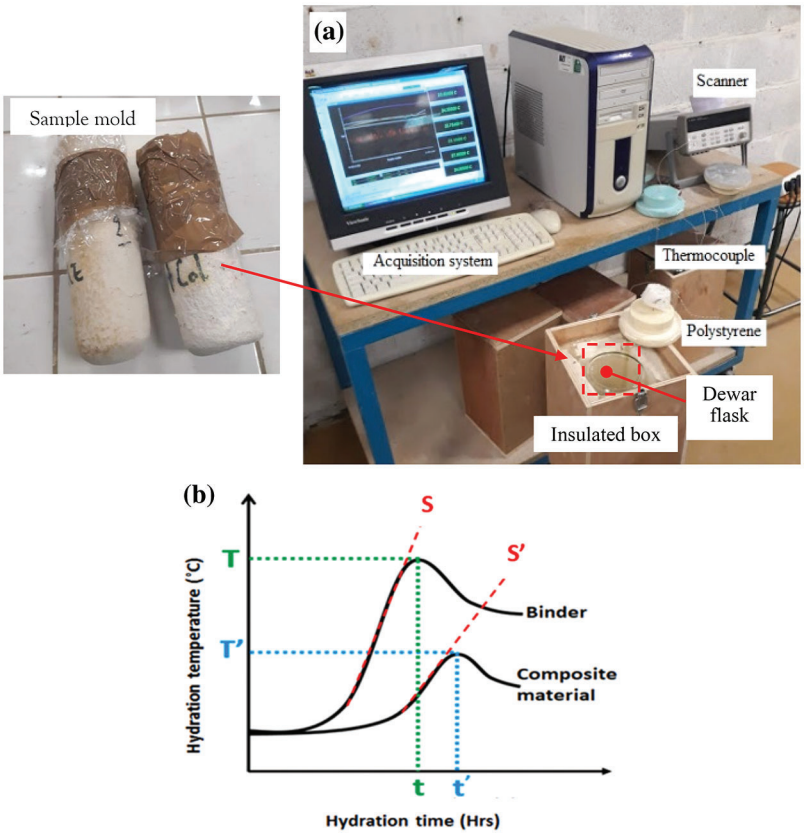

Figure 3: Hydration-test. (a): Hydration test set-up; (b): Schematic diagram of typical hydration curve [32]

The test was conducted by using 2 volumes of flax particles and 1 volume of binder-Aluminum-water mixture. After casting the fresh mixture in a specified mold, a thermocouple which serves to record the hydration temperature was inserted. After the mold being placed in a sealed flask, the hydration temperature was recorded along the time using a data acquisition system. To assess the effect of Aluminum, the specimen without Aluminum powder was also tested. The chemical compatibility level can be quantified by means the inhibitory index parameter I (%), using Eq. (3) [31,32].

$$I\ (\%) = \left(\frac{T - T'}{T}\right) . \left(\frac{t\prime - \mathrm{t}}{t}\right) . \left(\frac{S - S'}{S}\right) . 100 \tag{3}$$

where: T, T' **(°C)** are the maximum hydration temperatures of neat binder and the specimen-mix, respectively; t, t' (h) are the correspondent times to reach maximum temperatures, and S, S' (°C/h) are the maximum slopes of temperature-time curves for neat binder and specimen-mix, respectively.

However, the grade of inhibitory effect exerted by flax particles on binder hydration reaction is quantified through the Inhibitory index-value I (%). Table 4 reports the grade of inhibitory effect the smaller the I-value the higher the compatibility between binder and flax particles.

Table 4: Grade classification of inhibitory effect [32]

Inhibitory index I (%)	Inhibitory grade
I < 10	Low inhibition
10 < I < 50	Moderate inhibition
50 < I < 100	High inhibition
I > 100	Extreme inhibition

The fresh density of specimen, with different flax volume ratios, was measured after mixing procedure by filling container of 1 liter in volume. After the fresh specimen had reached a maximum volume increase corresponding to a duration time of 30 min, the expanded part was cut before weighing the sample.

After 28-day of curing time, physical properties of specimens containing different volumes of flax particles, including density, as measured by means weighting and dimensional measurements of cylindrical specimens with (110 × 220 mm) in sizes, and open porosity using Vacuum saturation protocol in accordance with Standard ASTM C20–00 [33], were investigated on (40 × 40 × 80 mm) prismatic sample. Before testing, all specimens were prepared by cutting the expanded part using circular saw with respect the initial molds dimensions as shown in Fig. 4a. The corresponding open porosity was calculated following Eq. (4):

$$\phi_P = 100\frac{M_{sat} - M_{dry}}{M_{sat} - M_{hyd}} \tag{4}$$

where: φ_P (%) is the open porosity; M_{dry}, M_{sat}, and M_{hyd} (kg) are the dry mass, saturated mass, and hydrostatic mass of the specimen, respectively.

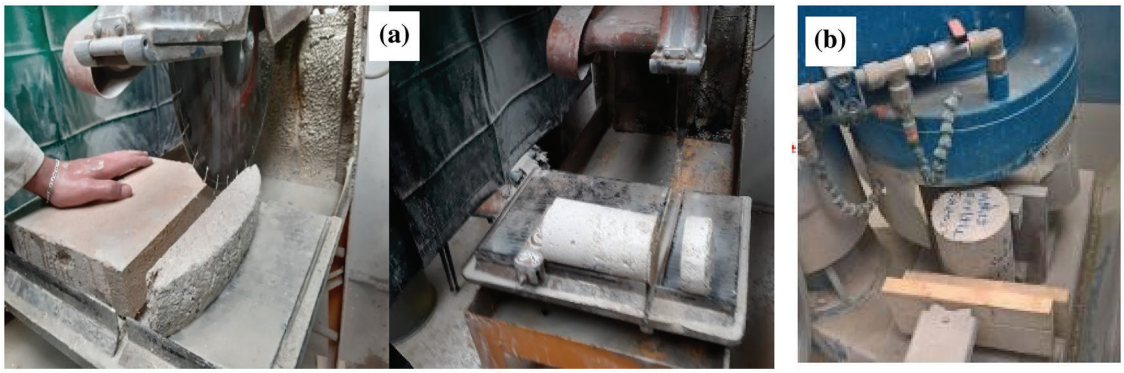

Figure 4: Specimen preparation before testing

The mechanical behavior was assessed through compressive and flexural-tests. The compressive-tests were performed on cylindrical samples measuring 110 × 220 mm in sizes, according to the European Standard EN 196-1 [34], using TINUS OLSEN H50KS electromechanical machine, with 50 kN in a maximum load capacity. Before testing, the lower and upper surfaces of each cylindrical specimen were leveled to ensure the high surfaces flatness (Fig. 4b). The tests were conducted under 4 mm/min in displacement control using two linear variable displacement transducers (Fig. 5a). For each composition-mix, three specimens are tested, while the average-value was reported. The average stress-strain diagram for all specimens was used to evaluate several derived parameters including compressive strength, ultimate strain, and the elastic modulus. The derived stress-strain values were determined according to Eqs. (5) and (6), while the elastic modulus was determined as the initial slope of the linear part of the stress-strain curve.

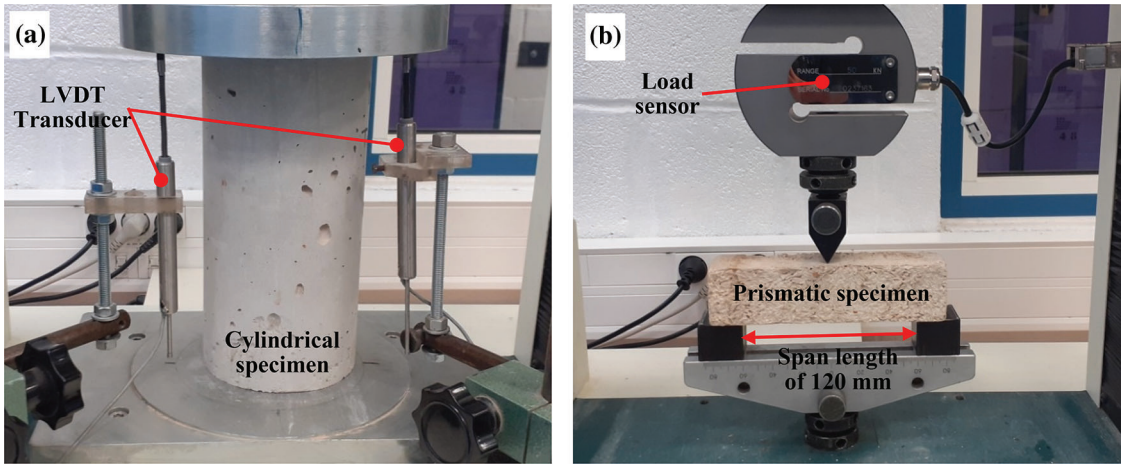

Figure 5: Mechanical-test machines. (a): Compressive-test; (b): Flexural-test

$$\sigma_c = \frac{F_{max}}{A} \tag{5}$$

$$\varepsilon = \frac{\Delta l}{l} \tag{6}$$

where: σ_c (MPa) is the compressive strength, F_{max} (N) is the maximum load at failure, A (mm^2) is the cross section of specimen, ε (mm/m) is the strain, Δl (mm) is the displacement, and l (m) the initial length of specimen.

The flexural-tests were performed on (40 × 40 × 160 mm) prismatic samples, using the same testing machine, according to the same standards EN 196-1 [34]. The tests were conducted with 1.2 mm/min of control deflection and of 120 mm in a span-value (Fig. 5b). The derived parameters including flexural strength, ultimate deflection, flexural elastic modulus, were evaluated through the average load-deflection curve of three tests for each composition-mix, according to Eqs. (7) and (8).

$$\sigma_f = \frac{3\ F_f.L}{2\ b.d^2} \tag{7}$$

$$E_f = \frac{k.L^3}{4\ b.h^3} \tag{8}$$

where: σ_f (MPa) is the bending stress; F_f (N) is the maximum load; L, b and d (mm) are the span of specimen in three-point bending-test, the thickness, and the average width, respectively; E_f (MPa) is the flexural modulus, k (N/mm) is the elastic stiffness of specimen, corresponding to the slope of the linear portion of load-deflection curve.

The change in failure mode of specimen with respect to flax amount was examined by evaluating the flexural toughness energy under loading. This parameter was estimated by evaluating the area under load–deflection diagram response up to post-cracking phase [35].

The thermal conductivity of samples was measured in dry state by using the Guarded Hot Plate method (GHP), according to the European Standard EN-12667 [36]. This method is considered as the most suitable due to its ability to measure thermal conductivity in a wide range from 0.02 to 5 W/m.K. The tests were performed using parallepipedic specimens with 250 × 250 × 50 mm in dimensions, which is placed between cooling plate and the heater plate. Passive protection zone surrounds the heat flow meter to prevent, as far as possible, lateral heat transfer. To perform the measurements at different temperatures, the temperatures of hot and cold plates are selected to obtain average temperature measurements of 10, 20, 30 and 40°C. The temperature gradient of the values through the sample is kept constant at 10°C during the tests. The device was equipped with thermocouple sensors and heat fluxmeter that are connected to the acquisition system which allows to record the temperatures and the dissipated heat. The (GHP) device and the sample preparation procedure are shown in Fig. 6.

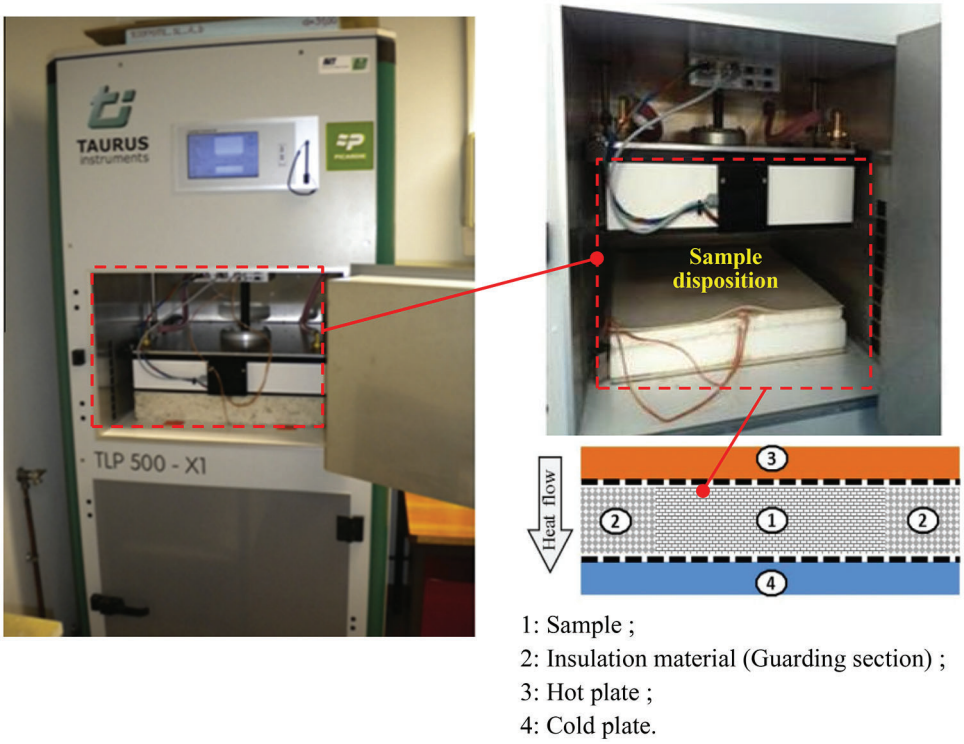

Figure 6: Guarded hot plate device (Taurus TLP 500) [36]

3 Experimental Results and Discussion

3.1 Fresh Sample-Properties

3.1.1 Chemical Compatibility

The inhibitory effect of flax particles on the binder hydration reaction, with and without Aluminum addition was assessed through recording of the variation in the hydration temperature of fresh specimen-mix along time, compared to that obtained for neat binder. The corresponding temperature-time curves are shown in Figs. 7 and 8, respectively, while the different parameters of binder hydration reaction are listed in Table 5. Results have shown that the addition of vegetable particles without Aluminum clearly inhibits binder hydration, as regards the decrease in maximum hydration temperature, with a longer time to reach a maximum temperature, as compared to the neat binder case. Table 5 shows that the maximum hydration temperature attained during hydration reaction mechanism decreased from 27.5°C to 24.3°C, while retarding the corresponding hydration time by 24 h. However, the addition of fax particles also results in increase of the initial hydration time from 1 h to 10.5 h, thus disturbs the hydration mechanism of binder. These results clearly show that the vegetable materials exerted an inhibitory effect on binder hardening, with a corresponding inhibitory index-value (I) of 15.5%, which classifies the effect as "Moderate" inhibition grade. According to several research-works, this incompatibility is attributed to the alkalis and dissolved components that inhibit specimen hardening [37,38]. The inhibition mechanism of hydraulic binder occurs when the calcium silicate hydrate nucleation sites on the originally positively charged surfaces are poisoned by the alkali inhibiter extractives including sugar acid anions, lignin, hemicellulose, etc., naturally contained in the vegetable materials.

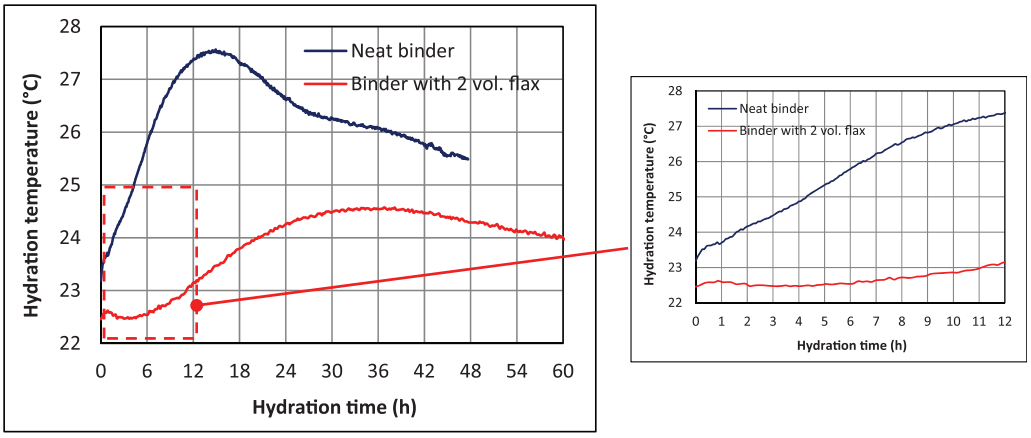

Figure 7: Effect of flax addition on temperature-time hydration curve of specimen without Aluminum powder

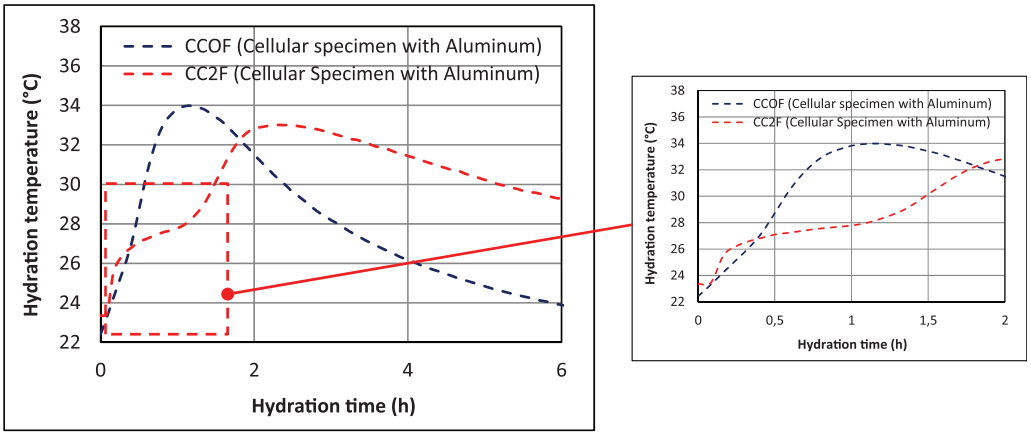

Figure 8: Effect of flax addition on temperature-time hydration curve of specimen with Aluminum powder

Table 5: Parameter-values of hydration-tests

Hydration parameters	Specimen			
	Neat binder	Binder with 2 vol. flax	CC0F (Cellular specimen with Aluminium)	CC2F (Cellular specimen with Aluminium)
Initial hydration time (h)	1	10.5	0.3	1.05
Max. hydration temperature (°C)	27.5	24.3	34	33
Time required for max temperature (h)	13.6	37.5	1.17	2.33
Hydration rate (°C/h)	0.45	0.11	16.47	7.7
Inhibitory index I (%)	–	15.5	–	1.55

The hydration-test carried for cellular specimen has shown that the addition of Aluminum powder leads to overcome the retardation of hydration reaction time observed bellow. This state is evidenced by a low initial binder hydration time, due to the chemical reaction occurred between Aluminum powder and

Calcium Hydrates. The hydration rate was highly enhanced, where the delay in sitting time of the binder is negligible. It results in a low inhibitory effect on the binder hydration, without a longer period for specimen hardening, which varied from 1.17 h to 2.33 h when flax particles were added. The corresponding inhibitory index-value of 1.55% classifies the mixtures as being of "low inhibition". According to the obtained results, it can be concluded that the flax particles do not exert inhibitory influence on the binder setting in the presence of Aluminium powder thus making the cellular specimen suitable for development. Hover, the use of Aluminum powder appears to significantly minimise the inhibitory effect exerted by vegetable materials.

3.1.2 Fresh Density of Cellular Specimen

The density-value of fresh cellular specimen, compared to that without Aluminum powder, for different flax volume ratios is shown in Fig. 9. It can be observed that the addition of flax particles from 0 to 2 in volume ratio leads to decrease fresh density from 1,300 à 910 kg/m^3, for cellular specimen, and from 1520 to 990 kg/m^3, for companion specimen without Aluminum addition. It can be observed that the lightening rate between cellular and non-cellular specimen with the same composition due to the Aluminum reaction decreased with increasing flax volume ratio. The corresponding lightening rate varied from 14.5% to 8.1%, for a flax volume ratio ranged from 0 to 2. The low efficiency of Aluminum addition to lightening specimen with increasing flax ratio in sample stems probably to the instability of generated air-bubbles in the binder matrix resulting from their collapse [39]. The reduction in air-bubble amount may be also related to the incomplete reaction of Aluminum powder due to the insufficient free Ca^{2+} ions due to their migration to cell walls and lumen cavity of flax particles, thus causing their mineralisation [40]. Fig. 10 shows the SEM micrographs of specimen microstructure, which highlighted the regular form of generated air-bubbles in the matrix of CC0F specimen with non-flax addition, without signs of bubbles collapse. In contrast, the addition of flax particles results in irregular form of air-bubbles size in the matrix, with a severe coalescence mechanism occurred.

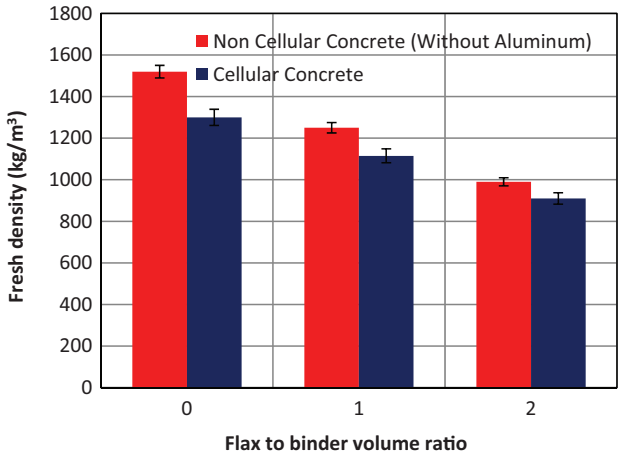

Figure 9: Fresh density-value of cellular and non-cellular specimen for different flax volume ratios

3.2 Hardened Sample Properties

3.2.1 Specimen Lightening

The effect of flax particle volume on dry density change of hardened cellular specimen is depicted in Fig. 11. Value decreased from 1,130 kg/m^3, for control specimen (0 volume of flax), to 670 kg/m^3 for specimen with 2 volumes of flax, corresponding to a reduction of up to 41%. The decrease in density is related to the physical properties of flax particles, since they exhibit low density, compared to the binder matrix. In addition, as shown in Fig. 10, the reaction between Aluminium powder and free Ca^{2+} ions

from Calcium Hydroxide creates porous structure that lightened the samples. As shown in Table 6, the test-results of porosity-values, measured using vacuum saturation procedure, indicated that the increase in flax particle volume increases porosity of specimen. The corresponding value varied from 28% to 69%. This contributes to lightening the specimen which make in the same magnitude of other Autoclaved Cellular Concrete specimen produced using different alternative materials (bottom ash, waste incineration particles, foaming activator, waste Aluminum, etc.) in term of density (300–800 kg/m^3), as reported in several research-works [41].

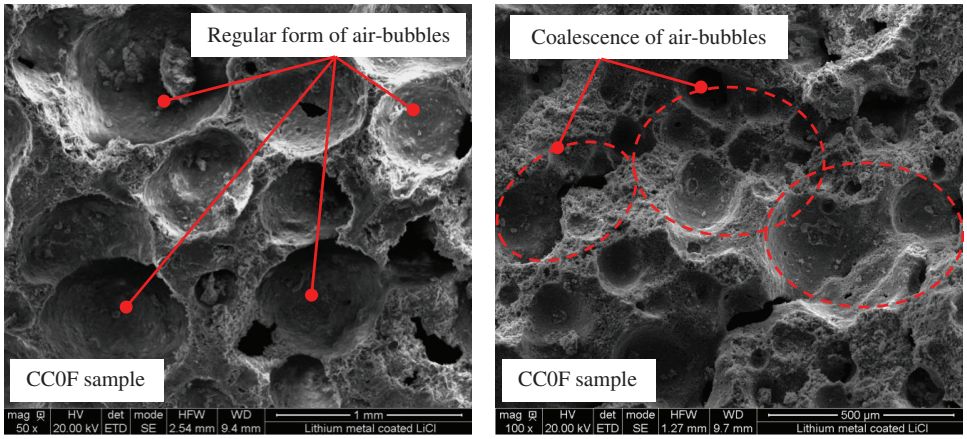

Figure 10: SEM micrographs of cellular specimen microstructure

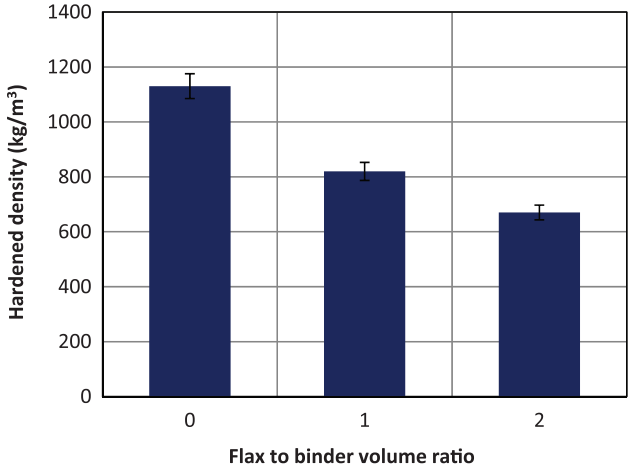

Figure 11: Hardened density-value of cellular specimen for different flax volume ratios

Table 6: Material properties in presence of 0.3% of Aluminum

Specimen ID	Dry density (kg/m^3)	Porosity (%)
CC0F	1,130 ± 15	42.8 ± 5
CC1F	820 ± 20	58.2 ± 6
CC2F	670 ± 25	67.1 ± 8

3.2.2 Mechanical Properties of Specimen

Compressive-Test Results:

The results of the change in 28-day compressive strength behaviour of specimen with respect to various flax volume ratios was assessed through stress-strain diagrams, as shown in Fig. 12. The results indicated that the increase of flax particles volume serves to decrease compressive strength from 1.52 MPa, for CC0F sample to 0.75 MPa for CC2F specimen with 2 volumes of flax, which corresponds to a reduction of approximately 50.6%. The strength defect of specimen is related to the mechanical properties of flax materials since they are less stiff than the surrounding binder matrix. The low stiffness of flax may be the predominant factor limiting the specimen mechanical properties, thereby resulting in defects at interfacial bond between particles and matrix. It is assumed that mechanical strength of specimen is opposite to its density. In addition, the porous structure leads to decrease compressive strength of sample. The more the air-bubble, the lighter the sample and the lower its mechanical strengths. In terms of bonding analyses, the SEM micrographs at Interfacial Transition Zone surface of particles-matrix are shown in Fig. 13. It can be clearly observed that flax particles–matrix bond appears to be lower, thus resulting in additional porosity which makes the specimen less resistant.

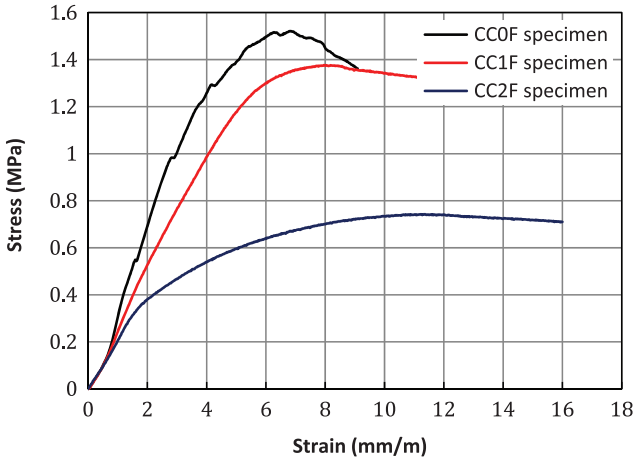

Figure 12: Stress-Strain diagram of specimens with different flax volumes

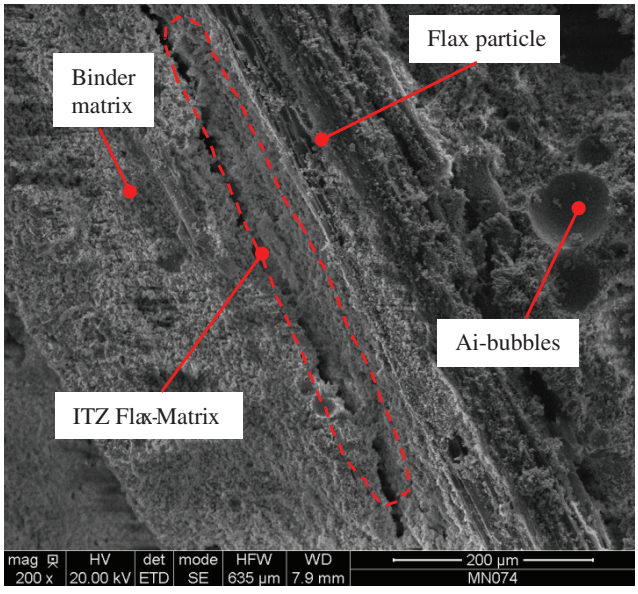

Figure 13: SEM micrograph of flax-binder matrix bond

However, the 28-day parameter-values of specimens when subjected to compressive test are shown in Table 7. The results highlighted the ductile behavior of specimen-based flax particles which exhibits high plastic phase and underwent significant deformation before failure, compared to the Control Specimen response. Results also show that the ultimate strain-value varied from 6.52 mm/m to 12.65 mm/m, where corresponding elastic modulus decreased from 353 to 205 MPa for CC2F sample. These results highlighted the effectiveness of flax addition in increasing elastic behaviour of sample. However, despite the decrease in compressive strength, the cellular specimen attains required substantial properties for using in a broad range of the cellular construction material applications, according to the RILEM "*Class III*" classification [42].

Table 7: 28-day parameter-values of compressive-tests

Specimen ID	Compressive strength (MPa)	Ultimate strain (mm/m)	Elastic modulus (MPa)
CC0F	1.52 ± 0.2	6.52 ± 0.4	353.00 ± 5
CC1F	1.30 ± 0.3	8.20 ± 0.6	262.24 ± 10
CC2F	0.75 ± 0.1	12.65 ± 0.9	205.00 ± 12

Flexural-Test Results:

The 28-days average results of flexural-tests depicted by the load-deflection diagrams of cellular specimens with different flax volumes are illustrated in Fig. 14, while the corresponding parameter-values like flexural strength, ultimate deflection, elastic stiffness, elastic modulus, and flexural toughness are reported in Table 8. Results indicated that addition of flax particles leads to decrease flexural strength from 1.10 MPa for Control Specimen to 0.65 for CC2F sample containing 2 volumes ratio of flax particles. This finding suggests that both mechanical properties of flax particles and sample's porous structure lead to decrease the mechanical strengths of specimen. Results also shown that for a given flax volume ratio, the reduction in flexural strength is lower than that obtained in compressive strength, due to the dilution effect of flax particles. The corresponding reduction rate in flexural strength is of up 41%. It is considered that the tension effect of the flax particles occurs during the diffuse micro-cracking phase of "bending" the active micro-cracks and then in delaying the onset of their appearance, which serves to improve specimen flexibility. This may also explained by the capability of flax particles to bridge the cracks and thus limiting their progression in the matrix. This bridge effect makes ductile specimen which exhibits a high deflection, compared to the Control specimen. The corresponding parameters reported in Table 8, show an increase in deflection of specimen, where the value varied from 0.358 mm to 1.044 mm when 2 volumes ratio of flax were added. The flexibility level of specimen containing flax particles was also characterised by the reduction in elastic stiffness, while the corresponding elastic modulus decreased from 234 MPa to 61.9 MPa, for CC2F sample.

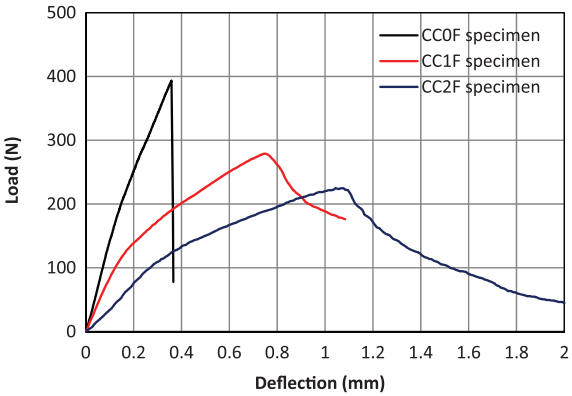

Figure 14: Stress-Strain diagram of specimens with different flax volumes

The effectiveness of adding flax particles to make specimen ductile may be analysed through the flexural toughness which gives a rise to evaluate the energy absorption capacity of specimen at post-cracking phase. As shown in Table 8, the increase of flax particles results in change of flexural toughness energy of specimen, where the variation of average-value from 80.1 10^{-3} J to 253.5 10^{-3} J evidences the ductile grade of cellular specimen. Fig. 15, which compares the shapes of specimens after failure, highlighted the bridging effect of flax particles thus allowing to control the rate of cracks propagation. In contrast to the control specimen which exhibited a sudden fracture followed by fast crack propagation, the addition of flax particles allowed the cellular sample to fail progressively and to maintain its structure due to the bridging action of flax particles. However, the post-cracking phase degree depends to the quality of the flax particle adherence to the binder matrix.

Table 8: 28-days parameter-values of flexural-tests

Specimen ID	Flexural strength (MPa)	Ultimate deflection (mm)	Elastic stiffness (N/mm)	Elastic modulus (MPa)	Flexural toughness (10^{-3} J)
CC0F	1.10 ± 0.2	0.358 ± 0.1	1,392.60 ± 30	235.00 ± 10	80.1 ± 10
CC1F	0.80 ± 0.3	0.751 ± 0.2	849.50 ± 45	143.35 ± 15	205.4 ± 25
CC2F	0.65 ± 0.2	1.044 ± 0.2	367.00 ± 50	61.90 ± 18	253.5 ± 40

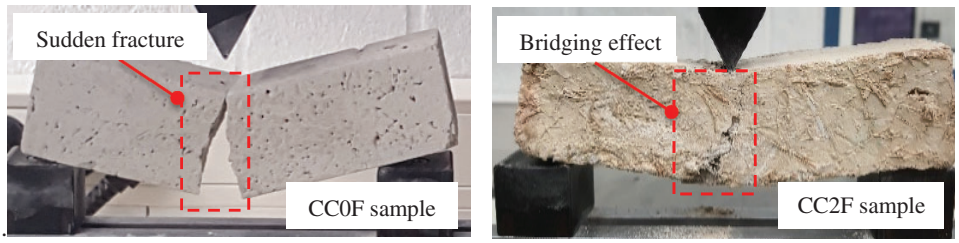

Figure 15: Shapes of cellular specimens after flexural failure

3.2.3 Thermal Conductivity of Specimen

The change in dry thermal conductivity of cellular specimen, with varying flax particle amounts, measured at different temperatures of 10, 20, 30, and 40°C, is shown in Fig. 16. The results clearly indicated the efficiency of flax particle addition in the increase of thermal performances of specimen. For temperature of 10°C, according to harmonised European standards of thermal conductivity measurement which must be determined at 10°C, the increase of the vegetable particles leads to decrease thermal conductivity-value from 0.354 W/m.K, for CC0F sample, to 0.163 W/m.K for CC2F. The decrease corresponds to approximately 54% lower, compared to the control specimen. The decrease in thermal conductivity of specimen is attributed to several factors, including its microstructure, material mixture proportioning, type of particles constituents, density, porosity, etc. The reduction in thermal conductivity of specimen is due the insulating effect of flax particles, which exhibited a lower thermal conductivity-value, compared to the lime-based binder matrix. It is evident from these results that the less thermal conductivity of particle addition produces the less conductive specimen. The porous structure of the cellular specimen will contribute to enhance the insulating property. However, the more the air-bubble, the lighter the specimen and the lower its thermal conductivity.

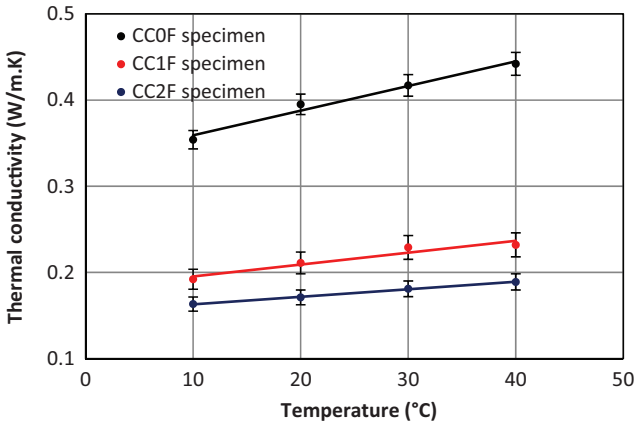

Figure 16: Dry thermal conductivity of cellular specimens with different flax volumes at different temperature

The investigation of specimen thermal conductivity, for temperature ranged from 10 to 40°C, shows a linear trend, where the increase in temperature results in a decrease of thermal performances of specimen. It results in an increase of thermal conductivity by 24.8% for CC0F and 15.7% for CC2F. These results evidenced that the thermal conductivity of specimen does not only depend on the conductive constituents, but it also on the porous structure of the samples. However, it well known that the raise in thermal conductivity of samples is also related to the increase in air conductivity with temperature. These results agree with that obtained by Omrani et al. [43] for composites based on Juncus fibers, showing that the thermal performances of specimen with high amount of Juncus fibers are less sensitive to the temperature increase, compared to the sample without fibers. However, based on the density range from 400 and 1,200 kg/m^3, it should be noted that the cellular specimens satisfy the basic requirement for use them as insulating-bearing materials, according the RILEM "*Class III*" specifications (compressive strength is above 0.5 MPa and thermal conductivity at 10°C less than 0.3 W/m.K [42].

Therefore, this research highlighted the benefits of adding flax particles to attain substantial properties of cellular specimen and allows considering a broad range in the cellular construction material applications.

4 Conclusion

Test program was conducted in this study to examine the potential use of flax by-product in preformulated Tradical PF70-based binder mixes to produce lightweight construction materials usable in cellular concrete applications. The specimen was lightened using Aluminum powder as a pore forming agent, which reacts with calcium hydroxide to form air-bubbles that lead to a porous structure. The fresh and hardened properties of specimen containing different volume ratios of flax particles were evaluated.

Results of tests performed at fresh state have shown that the use of Aluminum powder overcome the inhibitory effect that usually affect negatively the performances of specimen based vegetable materials. Therefore, the addition of Aluminum powder is an effective means leading to improve the binder hydration and the hardening of specimen. The examination of air-bubbles formation derived from reaction mechanism of Aluminum with Calcium Hydroxide has shown that the addition of higher amount of flax results their partial collapse.

Results-tests of hardened specimen have shown that the cellular specimen-based 2 volumes ratio of flax particles reached a dry density of 670 kg/m^3 with a compressive strength of 0.75 MPa. The compressive defect is evidenced by both low stiffness of particles and porous structure of the specimen. The reduction in flexural strength is lower than that in compressive strength due to the bridging effect of flax particle. The investigation of conductive property highlights the thermal performances of the material with a value

of 0.163 W/m·K in thermal conductivity. Although the strength was reduced, the cellular specimen satisfies the basic requirement for using as insulating-bearing wall, according to the RILEM "*Class III*" classification.

This research highlighted the effect of adding flax particles to attain substantial properties of innovative cellular materials and allows considering a broad range of applications in the cellular concrete field. In spite of the positive implications of the test-results, supplementary research is required to examine the effect of varying porous structure level on physico-mechanical and thermal properties of the specimen.

Funding Statement: The authors received no specific funding for this study.

Conflicts of Interest: The authors declare that they have no conflicts of interest to report regarding the present study.

References

1. EU Commision (2013). Trends to 2050. DOI 10.2833/17897.
2. González, M. J., Navarro, J. G. (2006). Assessment of the decrease of CO_2 emissions in the construction field through the selection of materials: Practical case study of three houses of low environmental impact. *Building and Environment, 41(7),* 902–909. DOI 10.1016/j.buildenv.2005.04.006.
3. Benmahiddine, F., Cherif, R., Bennai, F., Belarbi, T., Tahakourt, A. et al. (2020). Effect of flax shives content and size on the hygrothermal and mechanical properties of flax concrete. *Construction and Building Materials, 262,* 120077. DOI 10.1016/j.conbuildmat.2020.120077.
4. Brzyski, P., Barnat-Hunek, D., Suchorab, Z., Lagód, G. (2017). Composite materials based on hemp and flax for low-energy buildings. *Materials, 10(5),* 510. DOI 10.3390/ma10050510.
5. Trujillo, E., Moesen, M., Osorio, L., van Vuure, A. W., Ivens, A. et al. (2014). Bamboo fibres for reinforcement in composite materi*al*s: Strength Weibull analysis. *Composites Part A: Applied Science and Manufacturing, 61(2),* 115–125. DOI 10.1016/j.compositesa.2014.02.003.
6. Mulinari, D. R., Baptista, C. A. R. P., Souza, J. V. C., Voorwald, H. J. C. (2011). Mechanical properties of coconut fibers reinforced polyester composites. *Procedia Engineering, 10,* 2074–2079. DOI 10.1016/j.proeng.2011.04.343.
7. Al-Otaibi, M. S., Alothman, O. Y., Alrashed, M. M., Anis, A., Naveen, J. et al. (2020). Characterization of date palm fiber-reinforced different polypropylene matrices. *Polymers, 12(3),* 597. DOI 10.3390/polym12030597.
8. Saravana Kumar, M., Kumar, S. S., Babu, B. S., Chakravarthy, C. H. N. (2021). Influence of fiber loading on mechanical characterization of pineapple leaf and kenaf fibers reinforced polyester composites. *Materials Today: Proceedings, 46(23),* 439–444. DOI 10.1016/j.matpr.2020.09.804.
9. Chow, C. P. L., Xing, X. S., Li, R. K. Y. (2007). Moisture absorption studies of sisal fibre reinforced polypropylene composites. *Composites Science and Technology, 67(2),* 306–313. DOI 10.1016/j.compscitech.2006.08.005.
10. Ingrao, C., Giudice, A. L., Bacenetti, J., Tricase, C., Dotelli, D. et al. (2015). Energy and environment*al* assessment of industrial hemp for building applications: A review. *Renewable and Sustainable Energy Reviews, 51,* 29–42. DOI 10.1016/j.rser.2015.06.002.
11. Evrard, A., De Herde, A. (2009). Hygrothermal performance of lime-hemp wall assemblies. *Journal of Building Physics, 34(1),* 5–25. DOI 10.1177/1744259109355730.
12. Le, A. T., Gacoin, A., Li, A., Mai, T. H., El Wakil, N. (2015). Influence of various starch/hemp mixtures on mechanical and acoustical behavior of starch-hemp composite materials. *Composites Part B: Engineering, 75,* 201–211. DOI 10.1016/j.compositesb.2015.01.038.
13. Binici, H., Aksogan, O., Demirhan, C. (2016). Mechanical, thermal and acoustical characterizations of an insulation composite made of bio-based materials. *Sustainable Cities and Society, 20,* 17–26. DOI 10.1016/j.scs.2015.09.004.
14. Balčiūnas, G., Vėjelis, S., Vaitkusc, S., Kairytė, A. (2013). Physical properties and structure of composite made by using hemp hurds and different binding materials. *Procedia Engineering, 57,* 159–166. DOI 10.1016/j.proeng.2013.04.023.

15. Haik, R., Peled, A., Meir, I. A. (2020). The thermal performance of lime hemp concrete (LHC) with alternative binders. *Energy and Buildings, 210(5),* 109740. DOI 10.1016/j.enbuild.2019.109740.
16. Asli, M., Brachelet, F., Sassine, E., Antczak, E. (2021). Thermal and hygroscopic study of hemp concrete in real ambient conditions. *Journal of Building Engineering, 44(10),* 102612. DOI 10.1016/j.jobe.2021.102612.
17. Mazhoud, B., Collet, F., Prétot, S., Lanos, C. (2021). Effect of hemp content and clay stabilization on hygric and thermal properties of hemp-clay composites. *Construction and Building Materials, 300,* 123878. DOI 10.1016/j.conbuildmat.2021.123878.
18. Benmahiddine, F., Bennai, F., Cherif, R., Belarbi, R., Tahakourt, A. (2020). Experimental investigation on the influence of immersion/drying cycles on the hygrothermal and mechanical properties of hemp concrete. *Journal of Building Engineering, 32,* 101758. DOI 10.1016/j.jobe.2020.101758.
19. Araya-Letelier, G., Antico, F. C., Burbano-Garcia, C., Concha-Riedel, J., Norambuena-Contreras, J. (2021). Experimental evaluation of adobe mixtures reinforced with jute fibers. *Construction and Building Materials, 276(8),* 122127. DOI 10.1016/j.conbuildmat.2020.122127.
20. Saloni, A., Parveen, C., Lim, Y. Y., Pham, T. M. (2021). Influence of Portland cement on performance of fine rice husk ash geopolymer concrete: Strength and permeability properties. *Construction and Building Materials, 300(6),* 124321. DOI 10.1016/j.conbuildmat.2021.124321.
21. Sheridan, J., Sonebi, M., Taylor, S., Amziane, S. (2021). An investigation into the long-term carbonation of vegetal concretes containing a viscosity modifying agent. *Construction and Building Materials, 296(2),* 123765. DOI 10.1016/j.conbuildmat.2021.123765.
22. Zaid, I., Merzoud, M., Benazzouk, A. (2021). Morphological and mineralogical analysis of treated Diss fibers and their effect on physico-mechanical characteristics of Diss concrete based on alternative binder. *Construction and Building Materials, 307(85),* 124936. DOI 10.1016/j.conbuildmat.2021.124936.
23. Roy, A., Chakraborty, S., Kundu, S. P., Basak, R. K., Majumder, S. B. et al. (2012). Improvement in mechanical properties of jute fibres through mild alkali treatment as demonstrated by utilisation of the Weibull distribution model. *Bioresource Technology, 107(4),* 222–228. DOI 10.1016/j.biortech.2011.11.073.
24. Gill, A. S., Siddique, R. (2018). Durability properties of self-compacting concrete incorporating metakaolin and rice husk ash. *Construction and Building Materials, 176,* 323–332.
25. Walker, R., Pavia, S., Mitchell, R. (2014). Mechanical properties and durability of hemp-lime concretes. *Construction and Building Materials, 61(9),* 340–348. DOI 10.1016/j.conbuildmat.2014.02.065.
26. Wang, L., Lenormand, H., Zmamou, H., Leblanc, H. (2021). Effect of variability of hemp shiv on the setting of lime hemp concrete. *Industrial Crops and Products, 171(6),* 113915. DOI 10.1016/j.indcrop.2021.113915.
27. Blankenhorn, R. P., Blankenhorn, B. D., Silsbee, M. R., Dicola, M. (2001). Effect of fiber surface treatment on mechanical properties of wood-fiber cement composite. *Cement and Concrete Research, 31(7),* 1049–1055. DOI 10.1016/S0008-8846(01)00528-2.
28. Okino, E., de Souza, M. R., Santana, M. A. E., Alves, M. V., de Souza, M. E. et al. (2004). Cement bonded wood particle board with a mixture of eucalypt and rubberwood. *Cement and Concrete Composite, 26,* 729–734.
29. Qiu, J., Khalloufi, S., Martynenko, A., van Dalen, G., Schutyser, M. et al. (2015). Porosity, bulk density, and volume reduction during drying: Review of measurement methods and coefficient determinations. *Drying Technology, 33(14),* 1681–1699. DOI 10.1080/07373937.2015.1036289.
30. Tradical-BCB (2016). Chaux formulée pour Maçonner et Dégrossir et Bétons de Chanvre Tradical.
31. Moslemi, A., Garcia, J. F., Hofstrand, A. (2007). Effect of various treatments and additives on wood-Portland cement-water systems. *Wood and Fiber Science, 15(2),* 164–176.
32. Hofstrand, A., Moslemi, A., Garcia, J. F. (1984). Curing characteristics of wood particles from nine northern Rocky Mountain species mixed with portland cement. *Forest Products Journal, 34(2),* 57–61.
33. Raheem, Z. (2019). Standard test methods for apparent porosity, water absorption, apparent specific gravity, and bulk density of burned refractory brick and shapes by boiling water. ASTM C20-00(2010). DOI 10.1520/C0020-00R10.
34. van der Sloot, H. A. (2000). Comparison of the characteristic leaching behavior of cements using standard (EN 196–1) cement mortar and an assessment of their long-term environmental behavior in construction products

during service life and recycling. *Cement and Concrete Research, 30(7),* 1079–1096. DOI 10.1016/S0008-8846 (00)00287-8.

35. Deng, M., Han, J., Liu, H., Qin, M., Liang, X. (2015). Analysis of compressive toughness and deformability of high ductile fiber reinforced concrete. *Advances in Materials Science and Engineering, 2015(3),* 1–7. DOI 10.1155/2015/384902.
36. EN-12667 (2001). Thermal performance of building materials and products–determination of thermal resistance by the guarded hot plate method and the fluxmetric method–high and medium temperature resistance products.
37. Semple, K. E., Cunningham, R. B., Evans, P. D. (2002). The suitability of five Western Australian mallee eucalypt species for wood-cement composites. *Industrial Crops and Products, 16(2),* 89–100. DOI 10.1016/S0926-6690(02)00012-2.
38. Ajouguim, J., Page, S., Djelal, C., Waqif, M., Saâdi, L. (2021). Impact of Alfa fibers morphology on hydration kinetics and mechanical properties of cement mortars. *Construction and Building Materials, 293,* 123514. DOI 10.1016/j.conbuildmat.2021.123514.
39. Meyers, D. (1999). *Surfaces, interfaces and colloids: Principals and applications*. Second Edition. New York: Wiley-VCH.
40. Wei, J., Meyer, C. (2015). Degradation mechanisms of natural fiber in the matrix of cement composites. *Cement and Concrete Research, 73,* 1–16. DOI 10.1016/j.cemconres.2015.02.019.
41. Panesar, D. K. (2013). Cellular concrete properties and the effect of synthetic and protein foaming agents. *Construction and Building Materials, 44(6),* 575–584. DOI 10.1016/j.conbuildmat.2013.03.024.
42. Rilem, L. (1978). Functional classification of lightweight concrete. *Materials Structure, 11,* 281–283.
43. Omrani, H., Hassini, L., Benazzouk, A., Beji, H., ELCafsi, A. (2020). Elaboration and characterization of clay-sand composite based on Juncus acutus fibers. *Construction and Building Materials, 238(10),* 117712. DOI 10.1016/j.conbuildmat.2019.117712.